CI&CEQ
Chemical Industry & Chemical Engineering Quarterly

Available on line at
Association of the Chemical Engineers of Serbia *AChE*
www.ache.org.rs/CICEQ

Chem. Ind. Chem. Eng. Q. 25 (2) 193–206 (2019) CI&CEQ

VOJKAN D. RADONJIĆ[1]
JUGOSLAV B. KRSTIĆ[1]
DAVOR LONČAREVIĆ[1]
NIKOLA VUKELIĆ[2]
DUŠAN M. JOVANOVIĆ[1]

[1]University of Belgrade, ICTM, Department of Catalysis and Chemical Engineering, Belgrade, Serbia
[2]University of Belgrade, Faculty of Physical Chemistry, Belgrade, Serbia

SCIENTIFIC PAPER

UDC 66.094.25:665.347.8:544

Mg-Ni SUPPORTED ON PERLITE AS HYDROGENATION CATALYST: INFLUENCE OF Mg AND Ni CONTENT

Article Highlights

- Broken honeycomb-like perlite structure as catalyst support
- Morphological, textural, and structural characteristics of Ni and Mg influence
- Correlation between reducibility and hydrogen chemisorption
- Evaluation of lowest reduction temperature for catalyst preparation
- Catalyst behavior due to Ni and Mg influence in hydrogenation process

Abstract

Use of broken honeycomb-like expanded perlite as support for magnesium modified nickel catalysts in process of partial hydrogenation of sunflower oil was studied. By the use of the precipitation-deposition method, two groups of precursors were synthesized: different Ni/SiO_2 mole ratios with constant Mg/Ni mole ratio 0.1, and different Mg/Ni mole ratios with constant Ni/SiO_2 mole ratio 0.25. Characterizations of precursors were done (scanning electron microscopy, diffuse reflectance UV-Vis, infrared spectroscopy, N_2-physisorption, temperature programmed reduction (TPR) and He-pycnometry) to determine the material differences, considering the change in morphology, structure, texture and reducibility with overall Ni and Mg content. In addition, TPR and hydrogen chemisorption were performed in order to estimate the temperature reduction range of supported precursors and the dispersion degree of nickel in reduced precursors, respectively. The interaction between Ni^{2+} and perlite support was established. Different reducibility and dispersion were obtained as a function of Ni/SiO_2 and Mg/Ni mole ratios. After the precursor's reduction and paraffin oil impregnation, the obtained catalysts were tested in a sunflower oil hydrogenation reaction. Catalyst activity was monitored through the decrease of the refractive index and hydrogen consumption that gave the insight that the influence on catalyst activity represents the accessibility of triacylglycerols and not always the hydrogen determined dispersion degree.

Keywords: hydrogenation, magnesium, nickel catalyst, perlite, reduction.

Perlite is an amorphous volcanic glass, light gray, with SiO_2 composition higher than 70 wt.% and 2 to 5 wt.% of combined water. Commercially, the term perlite includes any volcanic glass that will exp- and dramatically, up to 20 times, when heated quickly, forming a lightweight frothy material [1,2]. Perlite has a significant applicability in construction industry, agriculture, and as an industrial filter aid, but there are just a few examples of its use as catalyst support [3-6].

Besides the direct use of vegetable oils in nutrition, the process of partial hydrogenation expands the area of their use. The partial hydrogenation of the vegetable oils continues to be applied in the modern chemical industry with the aim to decrease the unsaturation of the high fatty acids, to modify the physical

Correspondence: V.D. Radonjić, University of Belgrade, Institute of Chemistry, Technology and Metallurgy, Department of Catalysis and Chemical Engineering, Njegoševa 12, 11000 Belgrade, Serbia.
E-mail: vradonjic@nanosys.ihtm.bg.ac.rs
Paper received: 1 October, 2018
Paper revised: 1 November, 2018
Paper accepted: 15 November, 2018

https://doi.org/10.2298/CICEQ181001032R

properties of oils, and to enhance the oxidation and thermal stability of the hydrogenated products. The process is widely used in the production of margarines, cooking, frying and salad oils, chocolates, ice creams, shortenings and baking products [7-9].

Currently, metallic nickel (22-25 wt.% Ni) on different supports (silica, kieselguhr and alumina) represents the commonly applied commercial catalyst for the process of oil hydrogenation, due to its high activity, availability and low cost [10-12].

Supported nickel catalysts are usually prepared using different techniques like impregnation, ion exchange and precipitation-deposition with different precipitation agents [10,11]. The precipitation of nickel salt with sodium carbonate [13] in the presence of a silica slurry leads to the formation of nickel species like nickel basic carbonate and different nickel phyllosilicates. Obtained material can vary considerably with the changes in the precipitation conditions, synthesis temperature, textural characteristics of silica support, promotor species and nickel to silica ratio [14].

After precursor synthesis, in order to gain an active nickel catalyst, the nickel precursor must be reduced to metallic nickel [15]. The supported metal catalyst for oil hydrogenation is defined by the presence of highly dispersed metallic particles [16,17] on the support that are located in positions easily accessible to the molecules of triglycerides [18-21]. It is known that the nature and the organization of the supported phase influences the behavior of the precursors during the reduction pretreatment and contributes to the determination of size and dispersion of the metallic particles [10,22-25].

The aim of this work is to determine the use of broken honeycomb-like expanded perlite as support for active nickel-based catalysts modified with magnesium for hydrogenation of sunflower oil. Besides, the determination of influence with different nickel and magnesium content on morphology, structure, texture, and reducibility of catalyst precursors and their contribution on catalyst activity will be examined.

EXPERIMENTAL

Precursor preparation

Expanded perlite was supplied with the courtesy of Termika, Zrenjanin, Serbia (commercially denoted Perfit PF-295). Actually, PF-295 represents the finest fraction of expanded perlite that currently has no industrial use. The only laboratory pretreatment of PF--295 includes washing with distilled water at 90 °C for 30 min. Following, vacuum filtration with hot distilled water (≈80 °C) and drying in an oven at 110 °C for 24 h, the support was obtained (denoted PF). After microwave acid digestion of the support and ICP-OES measurements, chemical composition of the support was determined: SiO_2 = 74.1%; Al_2O_3 = 13.8%; Fe_2O_3 = 0.8%; K_2O = 4.6%; Na_2O = 3.6%; CaO = 0.7%; MgO = 0.1%, loss on ignition = 2.3%. All others chemicals used in precursor synthesis described in this paper are “proanalysis” purity grade.

The synthesis of precursors was performed in an externally heated PTFE reaction vessel equipped with a magnetic stirrer. The required volumes of the initial solutions of Mg and Ni nitrate salts, a concentration of 0.0583 and 0.5834 mol/dm^3, respectively, were transferred to the reaction vessel to obtain the corresponding mole ratio Mg and Ni (from 0.025 to 0.4). Solid anhydrous Na_2CO_3 was added at once, immediately after, and the resulting suspension was vigorously stirred and heated up to 90 °C. In all synthesis procedures, the amount of added Na_2CO_3 was 1.5 mole ratio towards Ni + Mg cations. After 30 min of precipitate aging, aqueous 2.0 wt.% suspension of PF, heated up to 90 °C, was added into the reaction vessel. The added mass of the prepared PF suspension enabled the obtaining of the predefined mole ratio of Ni:SiO_2 (from 0.25 to 1.75) in precursors. The obtained suspension was aged again for 30 min at the same temperature and stirring rate, after which it was vacuum filtered and thoroughly washed with hot (≈ 80 °C) distilled water until neutral pH. Filtrate was then resuspended in hot distilled water, washed and filtered again. Finally, precursors were dried in an air oven at 110 °C for 24 h, grounded to a powder, dried again and stored.

Two groups of precursors were synthesized. The first group is made out of five synthesized samples with constant magnesium to nickel mole ratio of 0.1 and different nickel to silica mole ratios of 0.25, 0.50, 0.75, 1.00 and 1.75. This group of precursors is labeled Mg-*x*Ni/PF where *x* represents Ni to SiO_2 mole ratio, and constant Mg to Ni ratio 0.1 is omitted. The second group was made out of six samples with constant nickel to silica ratio of 0.25 and different magnesium to nickel ratios denoted as 0.4, 0.2, 0.1, 0.05, 0.025 and 0. This group of precursors is labeled *y*Mg-Ni/PF where *y* represents Mg to Ni mole ratio and constant ratio Ni to SiO_2 0.25 is omitted. Also, the same synthesis procedure was done without the support to obtain nickel-magnesium basic carbonate denoted as Mg-NiBC and nickel basic carbonate without magnesium (NiBC).

Precursor characterization

The scanning electron microscopy observations were carried out on a JEOL JSM-6610LV microscope with a 20 kV beam.

A diffuse reflectance UV-Vis spectrum was obtained on a UV-Vis spectrophotometer (Evolution 500, Thermo Scientific), in spectral range of 250–800 nm. The results were presented in accordance with the Kubelka-Munk theory [26].

The infrared (IR) spectra of the samples, in the spectral range of 4000–400 cm^{-1}, with a resolution of a 2 cm^{-1}, were recorded using the KBr pellets technique: 1 mg of each sample is mixed with 200 mg of KBr (Nicolet 6700 FTIR, Thermo Scientific).

Textural parameters of support and precursors were obtained by N_2-physisorption at 77 K (Sorptomatic 1990, Thermo Finnigen) measurements. The obtained results were analyzed with a dedicated software package used for N_2 physisorption, ADP ver. 5.1 (Thermo Electron). Measurement accuracy of determining S_{BET} is approximately 2.8% [27].

Density measurements of support and precursors were performed by a helium gas pycnometer (Pycnomatic ATC, Thermo Scientific).

The temperature programmed reduction (TPR) of the precursors was performed (TPDRO 1100, Thermo Scientific). The TPR experiments were conducted using 4.9% H_2/Ar gas mixture with a flow rate of 20 cm^3 min^{-1}. The temperature was linearly raised from 50 to 900 °C at a heating rate of 10 °C min^{-1}; also, some measurements were performed at temperatures from 50 to 430 °C at a heating rate of 2 °C min^{-1}. The selected conditions were in the agreement with the criteria proposed by Monti and Baiker [28]. A cooling trap filled with CaO+NaO (Thermo Scientific) was installed between the oven and TCD to remove water and CO_2, formed during the reduction.

The hydrogen chemisorption measurements were carried out using pulse chemisorption on TPDRO 1100 instrument (Thermo Scientific) after reduction on chosen temperatures (270; 300; 330; 360; 460 °C) during 3 h, using 4.9% H_2/Ar gas with a flow rate of 20 cm^3 min^{-1} and heating rate of 2 °C min^{-1}. After reduction, the sorbed hydrogen was removed at the reduction temperature in flow of Ar for 1 h, cooling it in the same atmosphere, and after cooling the chemisorption was measured at 40 °C. The pulse chemisorption was performed with pure hydrogen after which the degree of dispersion was calculated [10,11,17].

Catalyst preparation and catalytic tests

The reduction of precursors was performed in a laboratory set-up using a quartz tube reactor by a procedure previously described [15]. In order to estimate the influence of reduction temperature on catalyst activity, selected precursor (Mg-0.25Ni/PF) was reduced at five different temperatures: 270, 300, 330, 360 and 390 °C. After reduction, reduced precursors were transferred to the beaker containing paraffin oil. During this process, the flow of argon in paraffin oil was continuously maintained. The impregnation procedure with Ar-purged paraffin oil was conducted in order to prevent oxidation of Ni^0 to Ni^{2+}, due to extreme pyrophoricity of metallic nickel in the presence of oxygen. After vacuum filtration of paraffin oil excess, the resulting catalysts were collected and stored in an Ar atmosphere.

The hydrogenation process was performed in a jacketed Parr Series 5100 (USA) glass reactor equipped with a computer-controlled mass flow controller F-201C and pressure meter F-502C (Bronkhorst). Hydrogen consumption during catalytic tests was obtained by integration of total consumed hydrogen during the process. As a starting material, commercially available edible sunflower oil was used (C16:0 = 6.9; C18:0 = 4.0; C18:1 = 26.0; C18:2 = 62.7) with iodine value of 131.7. After air evacuation with nitrogen gas, the reactor was connected to a hydrogen source and, during the process, H_2 pressure was maintained at a constant value of 0.2 MPa. Experimental conditions were: oil mass – 900 g; catalyst concentration – Ni related to the amount of oil as follows for different catalysts prepared; stirring rate – 1200 rpm; temperature – 160 °C.

Initial catalytic tests were performed for catalysts Mg-0.25Ni/PF prepared on different reduction temperatures (270-390 °C). After that, catalytic tests were made, using catalysts obtained from precursors of all mole ratios, Ni/SiO_2 and Mg/Ni at the selected reduction temperature (345 °C).

Catalytic tests, whose goal was to analyze the influence of reduction temperature of precursors on its activity, were performed at nickel to oil mass ratio of 0.03%, while catalytic tests where the analysis of nickel and magnesium influence was performed, nickel to oil mass ratio was 0.015%.

The refractive index values of crude oil (1.46371) and collected samples during the hydrogenation process were measured at exactly 50.00 °C (RX-5000α, Atago) and were used to monitor the hydrogenation process [29]. The fatty acid content of the starting oil, as well as the partially hydrogenated fatty acids, was determined by gas chromatograph Trace GC Ultra, equipped with FID and TriPlus autosampler (Thermo Scientific), previously described in detail [29].

RESULTS AND DISCUSSION

Characterization of precursors

In our previous work [30], regarding the possibility of using broken honeycomb-like expanded perlite as nickel catalyst support, it was shown that the material could be used as a catalyst support in the process of hydrogenation of sunflower oil. After precursor synthesis, color changes can be observed. Pale gray support, depending on nickel concentration, gains a pale green shade for precursors.

According to the chemical composition of precursors presented in Table 1, targeted Ni/SiO_2 and Mg/Ni mole ratios were achieved, for all precursors. Data accuracy of the obtained results in Table 1 is presented to the last significant figure. This confirms that all nickel and magnesium have been precipitated quantitatively, regardless of the composition and procedure of preparation. Packter and Uppaladinni also stated it for Ni, Mg precipitation with slightly different conditions without support [31]. Change in density of precursors is a direct consequence of the increase in nickel basic carbonate phase. As such, the density of precursors with a constant mole ratio of Ni and different Mg content (*y*Mg-Ni/PF serie) is not measurable, as the Mg content is almost negligible in comparison to Ni content.

SEM micrographs of the support PF, selected precursors series (Mg-*x*Ni/PF and *y*Mg-Ni/PF) and Mg-NiBC are shown in Figure 1.

On the perlite micrograph, sharp edged plates can be observed. Originally, expanded perlite grain has a honeycomb-like structure [32], although fine particle expanded perlite similar to Figure 1 is also reported [33,34] as a result of the brittle crushing of cell walls. Obviously, the plate form shape originates from the honeycomb structure due to the latter being broken during the thermal expansion of perlite. Broken honeycomb-like structure is not a disadvantage due to the fact that the open structure enables deposition of any species during precursor synthesis. That is demonstrated in Figure 1, where it can be clearly seen that the synthesis procedure leads to the formation of precursors with partially visible deposited nickel-magnesium species on the perlite support. Higher coverage of perlite support with nickel-magnesium agglomerates can be observed with nickel and/or magnesium content increase in precursors. On all precursor micrographs, similar sub-micron deposited species on perlite support form porous agglomerates of over-micron dimensions and are observable. The only considerable difference concerns the micrography of the 0.4Mg-Ni/PF sample with some lamellar shapes that may be a result of Mg contribution, which is higher for this precursor.

Diffuse reflectance UV-Vis spectroscopy has been used to further determine the precursor structure properties. Its spectrum contains two bands with maxima at 682 and 399 nm (Figure 2). These bands are typical of Ni^{2+} ions in octahedral geometry assigned to the transitions $^3A_{2g} \rightarrow {}^3T_{1g}(F)$ and $^3A_{2g} \rightarrow {}^3T_{1g}(P)$ [35].

Regardless of possible causes of band ratio change in the spectra, the origin of the two most intensive bands in the precursors is known. These bands originate from spin-orbital transitions: $^3A_{2g}(F) \rightarrow {}^3T_{1g}(P)$ for lower wavelength and $^3A_{2g}(F) \rightarrow {}^3T_{1g}(F)$ for higher wavelength, which are associated to the octahedral structural coordination of Ni^{2+} [36–39]. Commonly, besides the absorption bands that origin-

Table 1. Measured concentrations of Ni and Mg, obtained mole ratios and sample densities

Serie	Precursor	Ni, %	Mg[a], %	*n*Ni/*n*SiO_2 ratio	*n*Mg/*n*Ni ratio	Density, g/cm^3
	PF	0.00	0.06	0	-	2.23
	Mg-NiBC	51.64	2.14	-	0.100	3.62
Mg-*x*Ni/PF	Mg-0.25Ni/PF*	13.64	0.56	0.25	0.099	2.72
	Mg-0.50Ni/PF	21.57	0.90	0.50	0.101	2.86
	Mg-0.75Ni/PF	26.75	1.11	0.75	0.100	2.92
	Mg-1.00Ni/PF	30.21	1.25	1.00	0.100	3.00
	Mg-1.75Ni/PF	35.98	1.49	1.75	0.100	3.07
*y*Mg-Ni/PF	0Mg-Ni/PF	13.92	0.00	0.25	0.000	2.72
	0.025Mg-Ni/PF	13.73	0.14	0.25	0.025	2.72
	0.05Mg-Ni/PF	13.64	0.28	0.25	0.050	2.72
	0.1Mg-Ni/PF*	13.64	0.56	0.25	0.099	2.72
	0.2Mg-Ni/PF	13.41	1.11	0.25	0.200	2.72
	0.4Mg-Ni/PF	13.10	2.17	0.25	0.400	2.72

[a]Magnesium content present in PF is subtracted from total precursors magnesium content. *Note that samples Mg-0.25Ni/PF and 0.1Mg-Ni/PF are one and the same

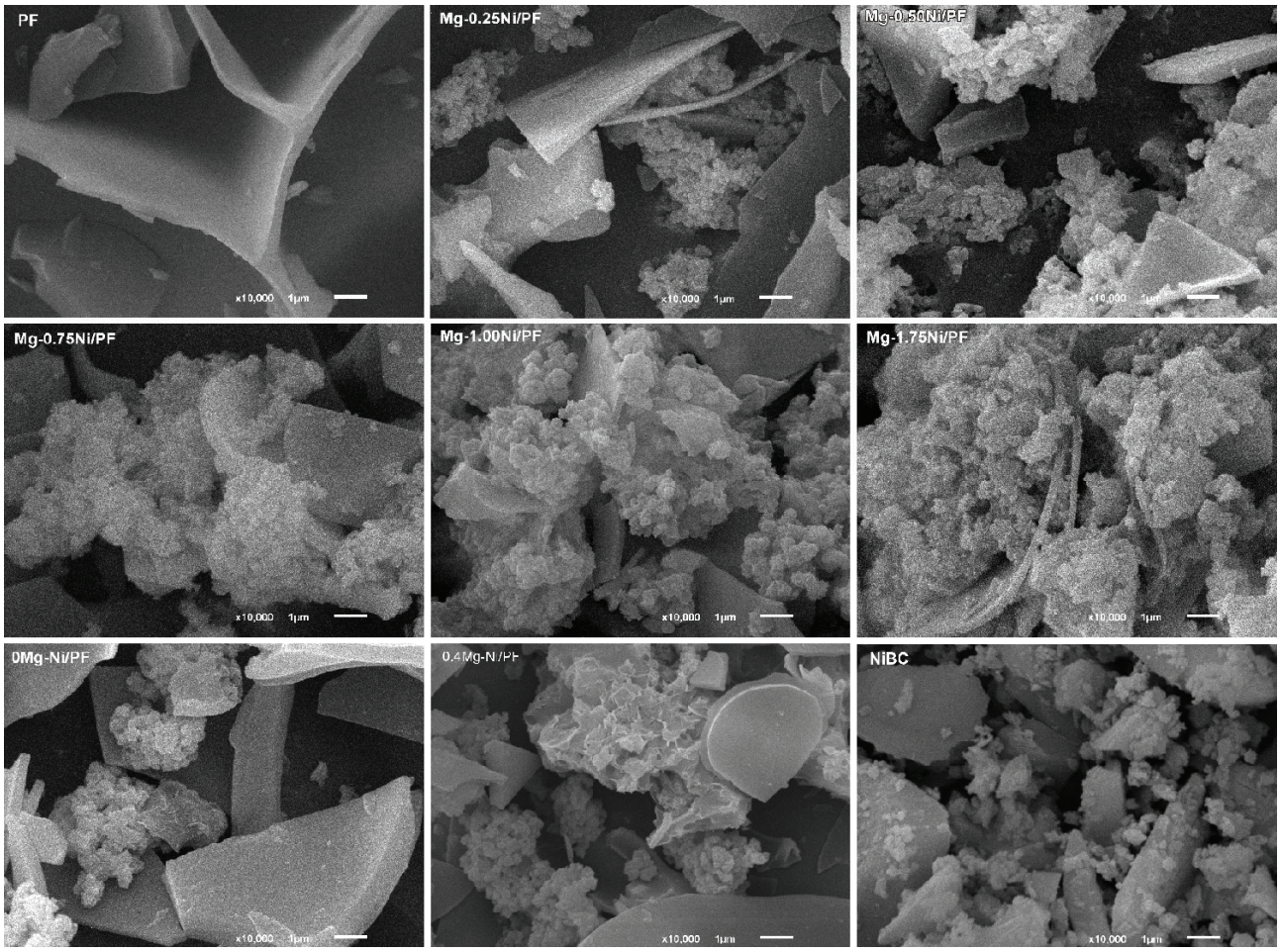

Figure 1. SEM micrographs of selected samples: PF; Mg-0.25Ni/PF; Mg-0.50Ni/PF; Mg-0.75Ni/PF; Mg-1.00Ni/PF; Mg-1.75Ni/PF; 0Mg-Ni/PF; 0.4Mg-Ni/PF; NiBC (magnification of x10 000 and tick bar 1μm).

ate from allowed transitions, spectra can show the absorption bands of weak intensity that can be attributed to the spin-forbidden transitions (triplet to singlet): $^3A_{2g}(F) \rightarrow {}^1E_g(F)$ [38]. Complex band structure on the position of higher wavelength, which actually consists of two overlapping bands of similar intensity at approximately 682 and 747 nm is proof of their existence.

It is inevitable that the influence of ligands is noticeable in bathochromic and hypsochromic shifts of bands maxima [36,38]. Due to that, in precursor spectra, nickel is in an octahedral structure with ligands that are causing the hypsochromic shift of lower wavelength maxima in DR UV-Vis spectra (399→391 nm), clearly seen in the spectra of lower nickel concentrations (with the Ni/SiO_2 mole ratio below 1.00) in comparison with the spectra of Mg-NiBC. This shift can originate by substituting one or more water molecules or CO_3^{2-} and OH^- anions with a silanol group, therefore bonding with the silica structure [37]. The influence of the ligand structure is less pronounced at higher wavelength transitions and is then not noticeable as a shift in the spectrum.

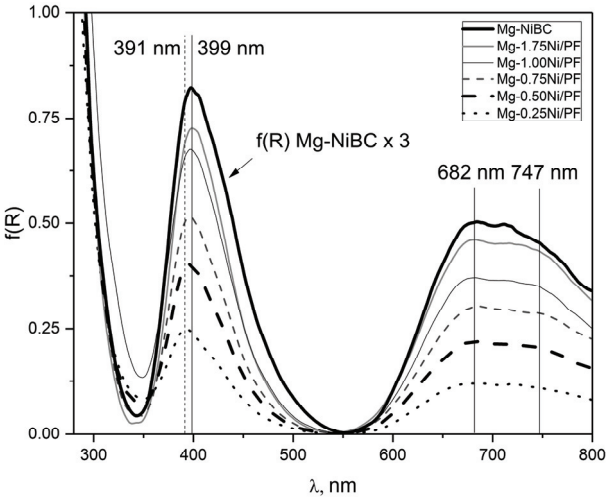

Figure 2. DR-UV-Vis spectra of synthesized samples.

Infrared spectra of PF, Mg-NiBC and all synthesized precursors are presented in Figure 3a and b. Prepared PF in the spectral region of 500 to 1500 cm^{-1} shows a wide band at about 1049 and 1150 cm^{-1}. These two bands can be recognized in all aluminosilicate IR spectra and are attributed to Si-O-R stretching vibrations, where R can be Al or Si. The band at 791 cm^{-1} is attributed to symmetric stretching of ≡Si-O-Si≡ that has a shoulder at 723 cm^{-1} which can be attributed to symmetric stretching of Si-O-Al [40]. The weak wide band at around 570 cm^{-1} also originates from symmetric stretching of Si-O-Al [40]. The band around 455 cm^{-1} can be associated to the bending vibration of Si-O-Si or O-Si-O.

Basic nickel carbonate (Mg-NiBC) has typical bands assigned to the carbonate anions around 1452, 1384 and 827 cm^{-1} [22]. The well-expressed bands at 1452 and 1384 cm^{-1} in the IR spectrum of all precursors are attributed to the presence of an additional carbonate-containing phase, located on the support surface seen in SEM micrographs. In all spectra of precursors, the broad asymmetric band below 3700 cm^{-1} with a minimum at around 3440 cm^{-1}, is attributed to the stretching vibrations of hydrogen bonds of -OH. In addition, the existence of the band at 1630 cm^{-1} confirms the presence of physisorbed water on the precursor's surface [22,39].

The most obvious differences in the IR spectra of precursors are the decreases in band intensity of Si-O-R stretching vibrations region as nickel-magnesium species increase. At the same time, the bands that originate from carbonate increase. However, comparing bands in the lower wavenumber region obtained in synthesized precursors may offer evidence of created Ni^{2+} species on the support surfaces. On Mg-NiBC spectra, existence of a broad asymmetric band at 685 cm^{-1} is evident. This band also exists in spectra of precursors, although slightly shifted towards lower wavenumbers with a minimum at around 656 cm^{-1}. Although this band is broad and weak in intensity, the shift may indicate Ni species interaction with the support, compared to the unsupported Mg-NiBC sample, most likely to Ni-O-Si vibrations [41]. This type of support interaction will have to have an influence on precursor reducible properties, which will be analyzed afterwards.

Observing the IR spectra of precursors with different magnesium content and constant Ni to SiO_2 mole ratio does not show any significant influence on intensity and position of bands (Figure 3b). Although the band at 1380 cm^{-1} originates from nickel basic carbonate-like species, it seems to be less expressed in precursors with higher amounts of Mg, typically for 0.2Mg-Ni/PF and 0.4Mg-Ni/PF.

Adsorption-desorption isotherms of samples are shown in Figure 4a and b and the results of calculated textural parameters are given in Table 2. According to the IUPAC classification of N_2 physisorption isotherms of the perlite support is Type III, characteristic for weak adsorbate-adsorbent interactions and is associated with nonporous adsorbents [42]. Small values of total pore volume (V_{tot}), specific surface area (S_{BET}) and BET constant (C_{BET}) confirm a nonporous nature of the support. Isotherm of nickel basic carbonate (Mg-NiBC) is type Ib (characteristic for microporous materials) with certain elements of type IV (typical for mesoporous materials). Indeed, a sharp vertical increase of adsorbed volume in the smallest relative pressure region confirms a system of micropores (pore width ≤ 2 nm), while the long transition region has a constant increase of adsorbed volume ending in the mesoporous region (p/p_0 ≈ 0.6) thus confirming the existence of mesopores not larger than 6 nm.

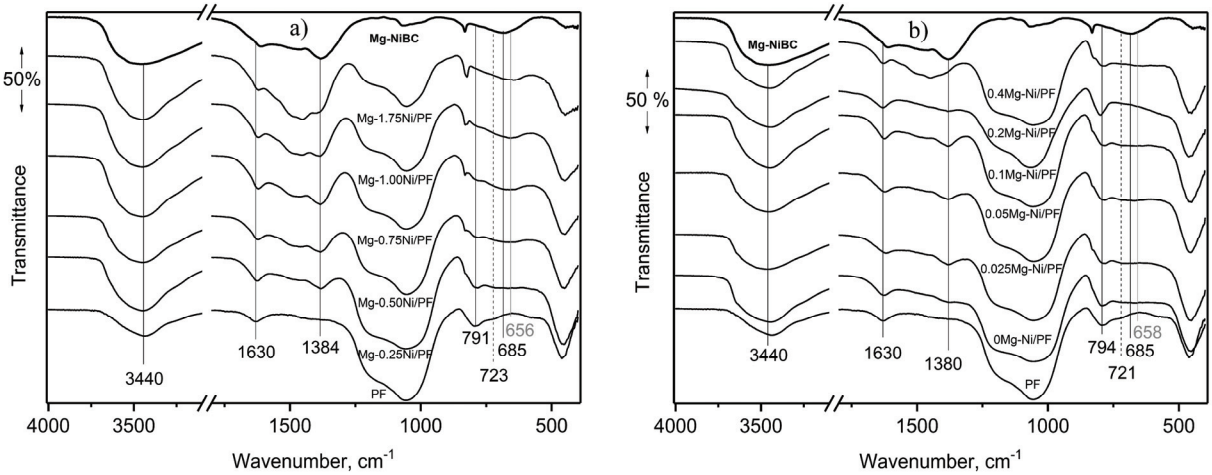

Figure 3. Infrared spectra of: a) precursors with different amount of Ni content and b) precursors with different amount of Mg content.

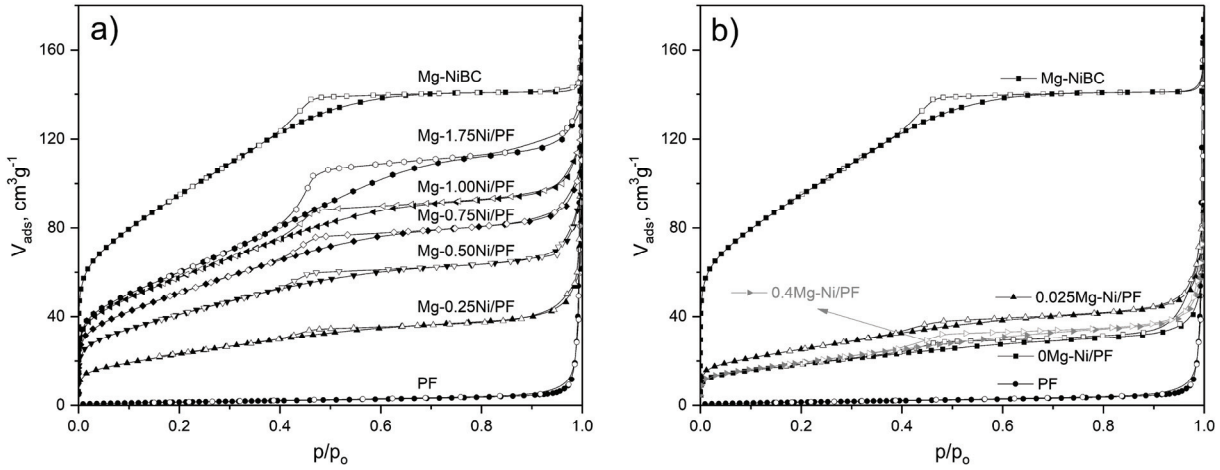

Figure 4. N_2 physisorption at 77 K of: a) precursors with different amount of Ni content and b) selected precursors with different amount of Mg content.

The precursor isotherm type has significantly changed, compared to the support, and all of the precursors can be classified as type IIb with the H3 hysteresis, characteristic for aggregates of plate-like particles with non-rigid slit-shapes [42]. This is a contribution of the formation of Ni^{2+} species, assured through the constant increase in total pore volume (Figure 4a) and almost linear increase of S_{BET} as a function of nickel concentration in precursors (constant mole ratio of Mg/Ni = 0.1). On the other hand, V_{tot} values in the precursor series with variable mole ratio of Mg/Ni (Figure 4b) are barely noticeable and have a tendency to decrease as Mg concentration increases in the precursors. Isotherms of these series take the same position in whole p/p_0 range, which is why isotherms of 0.05Mg-Ni/PF and 0.2Mg-Ni/PF are omitted in Figure 4b. The fluctuating tendency of S_{BET} for this series indicates a complex interaction mechanism as the Mg concentration increases in precursors possibly by both isomorph substitution of Ni^{2+} with Mg^{2+} and accumulation of magnesium basic carbonate on the nickel phase [31,43,44]. It is undeniable, however, that Mg content above 0.56% in precursors (nMg/nNi above 0.1) causes a decrease in specific surface area of precursors.

Some insight and information about the influence of the support and Mg can be obtained by analyzing Mg contribution in synthesized nickel basic carbonate and precursor with and without Mg. For example, the specific surface area of Mg-NiBC (nMg/nNi = 0.1) is 10% higher than in NiBC (347 *vs.*314 m^2/g). At the same time, the precursor with Mg (13.64% Ni and nMg/nNi = 0.1) has a specific surface area almost 29% higher than the precursor without

Table 2. N_2 physisorption results of all precursors

Sample	V_{tot}[a], cm^{3}g^{-1}	V_{mic}[b], cm^{3}g^{-1}	V_{meso}[c], cm^{3}g^{-1}	S_{BET}[d], m^2/g	C_{BET}	Ni, %
PF	0.019	0.002	0.015	6	18	0
Mg-NiBC	0.218	0.115	0.132	347	78	51.64
Mg-0.25Ni/PF	0.080	0.028	0.054	86	64	13.64
Mg-0.50Ni/PF	0.121	0.051	0.082	149	87	21.57
Mg-0.75Ni/PF	0.146	0.063	0.103	186	74	26.75
Mg-1.00Ni/PF	0.167	0.071	0.121	210	82	30.21
Mg-1.75Ni/PF	0.195	0.073	0.154	221	70	35.98
0Mg-Ni/PF	0.065	0.024	0.039	66	113	13.92
0.025Mg-Ni/PF	0.086	0.032	0.052	92	95	13.73
0.05Mg-Ni/PF	0.082	0.028	0.049	79	99	13.64
0.1Mg-Ni/PF	0.080	0.028	0.054	86	64	13.64
0.2Mg-Ni/PF	0.080	0.026	0.054	78	63	13.41
0.4Mg-Ni/PF	0.072	0.024	0.052	70	85	13.10

[a]Total pore volume calculated by Gurvich at $p/p_0 = 0.98$; [b]Micropore volume calculated by Dubinin and Raduskevich method; [c]Mesopore volume calculated by Dollimore and Heal method; [d]Specific surface area calculated by Brunauer-Emmett-Teller method

Mg (86 *vs.* 66 m^2/g). Obviously, besides Mg contribution, perlite support encourages dispersion of nickel species even significantly, most probably by preventing the formation of large aggregates.

Temperature programmed reduction and chemisorption measurements

Reducibility of the precursors is investigated by TPR technique and the results are shown in Figure 5a (different amount of nickel and constant Mg/Ni ratio) and b (different amount of magnesium and constant Ni/SiO_2 ratio). Also, TPR profile of Mg-NiBC is presented in order to elucidate the effect of nickel and magnesium loading in the precursor on their reduction properties.

Although the TPR profiles were measured in the region 50-900 °C, profiles are shown only in the temperature region where the visual changes in profiles occur (200-700 °C).

The reducibility of the unsupported Mg-NiBC is attested by the single symmetric peak in the region 250-400 with T_{max} at 310 °C that is assumed to represent the full reduction of bulk Ni^{2+} ions to Ni [22]. Precursor for the series with a different amount of nickel, TPR profiles show almost the same tendency in the slightly shifted region, starting reduction process at 270 °C and, because of their asymmetry (T_{max} = 314 °C), ending at above 400 °C. TPR profiles of Mg-0.25Ni/PF and Mg-0.50Ni/PF have a prolonged reduction tail up to T = 600 °C that is most probably caused by nickel-support interaction. For the highest nickel concentration (Mg-1.75Ni/PF), a shoulder on TPR profiles appears ($T \approx$ 330 °C), indicated with an arrow in Figure 5a because of overlapping nickel species that are interacting with the support and non-interacting NiBC species. As the amount of unsupported NiBC species increases, this shoulder becomes more noticeable.

By comparing the TPR profiles of Mg-NiBC and Mg-0.25Ni/PF (Figure 5a), the information about the contribution of perlite support can be recognized. Asymmetrical profile of Mg-0.25Ni/PF towards higher temperatures, which does not exist in the TPR profile of NiBC, indicates the existence of interaction of Ni^{2+} species with PF support to some extent.

Introducing even the smallest amount of Mg into the system (0.025Mg-Ni/PF *vs.* 0Mg-Ni/PF) results in a change of the TPR profile, increasing its tailing in the high temperature region as the Mg amount increases. Obviously, the Mg introduction into the system hinders the reduction of precursors. The TPR profiles change significantly as the Mg/Ni mole ratio exceeds 0.1. The shift of T_{max} to 325 °C for 0.2Mg--Ni/PF and even a complete change in profile for 0.4Mg-Ni/PF (T_{max} = 342 °C, high temperature shoulder at 410 °C and a prolonged tail, up to 700 °C) is evident.

It is well known that there is a connection between reduction conditions and catalyst activity [45,46]. Therefore, the chemisorption measurements were carried out after precursors were reduced at the same heating rate used for catalyst preparation (2 °C/min). Changing the heating rate from 10 to 2 °C/min causes a maximum position shift towards lower values for ≈25 °C (Figure 5a).

In order to establish the influence of maximum reduction temperature on nickel dispersion degree, a temperature range from 270 to 460 °C was chosen (Table 3). It is worth mentioning that the complete reduction of Ni^{2+} species does not necessarily mean that the catalyst will be active, due to the possibility of

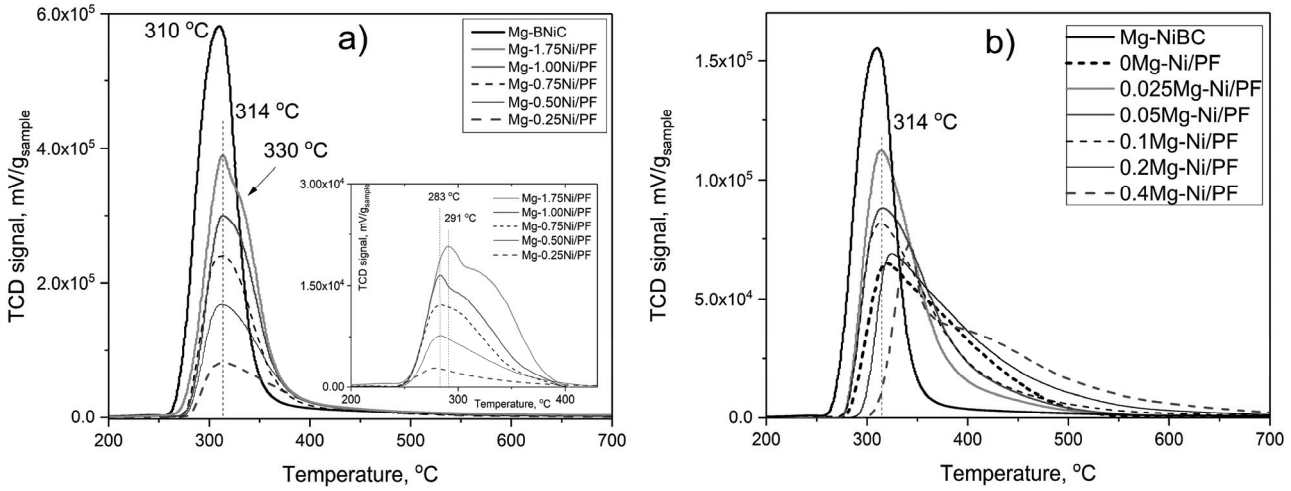

Figure 5. TPR profiles of: a) precursors with different amount of Ni content (insert reduction heating rate 2 °C/min) and b) precursors with different amount of Mg content.

nickel crystalline growth through aggregation, which therefore decreases the number of active Ni sites on the support, resulting in the overall decrease of catalyst activity.

Obtained dispersion degrees can be analyzed as influences of the reduction temperature, nickel and magnesium content. By observing the temperature influence, starting from 270 °C, the decrease in metal dispersion is clearly seen as the reduction temperature increases for samples with higher nickel content (Mg-0.75Ni/PF, Mg-1.00Ni/PF and Mg-1.75Ni/PF). Samples with nickel content smaller than 26.75% (Mg-0.25Ni/PF, Mg-0.50Ni/PF) do have a small, but not insignificant, increase in metal dispersion at 300 °C, followed by the same decrease in dispersion degree as the reduction temperature continues to increase. This occurrence can be associated with the existence of different nickel species: one that is generated through the interaction of basic nickel carbonate with the support surface and other noninteracting basic nickel carbonate, positioned and placed above the first one. As the nickel content in the precursor increases, the interaction with the support is less pronounced because of the increasing amount of noninteracting nickel basic carbonate species. The mechanism of the reduction process goes from the surface nickel species down to the inner nickel species so the dispersion of nickel, therefore, depends on all species present in precursors and also their ratio, as well as their position. This is the reason why, in the precursors with low Ni contents (Mg-0.25Ni/PF, Mg-0.50Ni/PF), dispersion increases as reduction temperature increases to 300 °C; the contribution of the bound species (that are more difficult to reduce at 270 °C) is somewhat higher and with the increase of the reduction temperature are noticeable and contribute to the overall dispersion. For other precursors with higher nickel content, reduction of species on the surface of the support is difficult due to their overlapping with the noninteracting nickel basic carbonate support. By increasing the temperature, the content of reduced nickel increases in depth, but it does not contribute to the dispersion increase. On the contrary, the possible interactions of Ni aggregates lead to their growth, contributing to the overall decrease of dispersion values. Finally, when the temperature is sufficient to reduce the layers of Ni^{2+} species bonded to the support, the total change of dispersion continues to decrease due to the higher contribution of Ni^0 aggregates growth. It is worth noting that the mechanism of Ni aggregates growth is not questionable, especially when the low values of dispersion for the highest analyzed reduction temperature (460 °C) is taken into account.

The dispersion results of the magnesium-unmodified nickel basic carbonate samples with and without the perlite support, also confirms the existence of interaction between nickel basic carbonate and support surface. The sample of nonsupported nickel basic carbonate without magnesium has nickel dispersion less than 0.1%, while the precursor without magnesium on a perlite support (0Mg-Ni/PF) obtained at the same reduction conditions (T = 300 °C) has Ni dispersion of 7.7%. This is a consequence of Ni^{2+} species interaction with perlite surface in the precursor. Interestingly, in the sample without perlite support, the contribution solely of Mg on the increase of nickel dispersion is also significant. The sample of non-supported basic nickel carbonate with magnesium (nMg/nNi = 0.1) reduced at T = 300 °C, has nickel dispersion of 5.0%. The surprisingly high dispersion degree of this sample can be interpreted as

Table 3. Metal dispersion degree for all samples

Sample	Ni, %	Reduction temperature, °C					
		270	300	330	345	360	460
		Metal dispersion, %					
0Mg-Ni/PF	13.92	6.9	7.7	7.8	7.3	6.4	
Mg-0.25Ni/PF	13.64	10.1	10.3	9.6	9.2	8.4	4.9
Mg-0.50Ni/PF	21.57	10.2	10.8	10.0	8.7	7.2	5.6
Mg-0.75Ni/PF	26.75	9.6	8.7	8.3	7.2	6.0	4.7
Mg-1.00Ni/PF	30.21	9.7	8.6	8.3	8.2	7.7	4.6
Mg-1.75Ni/PF	35.98	9.8	9.5	8.4	8.2	7.6	4.9
0.025Mg-Ni/PF	13.73		7.4	6.5	5.9	5.0	
0.05Mg-Ni/PF	13.64		8.5	7.0	7.0	6.9	
0.1Mg-Ni/PF	13.64	10.1	10.3	9.6	9.2	8.4	4.9
0.2Mg-Ni/PF	13.41		8.8	9.7	9.8	9.9	8.7
0.4Mg-Ni/PF	13.10		3.4	9.2	10.0	10.1	8.1

altering the structure and/or dividing nickel basic carbonate structure, thus hindering Ni^0 particle aggregation. More importantly, the introduction of Mg into the system (0Mg-Ni/PF vs. Mg-0.25Ni/PF) leads to a further increase of dispersion degree by 34% (7.7% *vs.* 10.3%), as a result of Mg^{2+} influence on the nickel species, already observed through the change of the TPR profiles.

The influence of magnesium on nickel dispersion is also a function of reduction temperature. For low reduction temperatures (270 and 300 °C) and mole ratio Mg to Ni ≤ 0.1, as Mg concentration increases, the dispersion of nickel in precursors also increases. On the other hand, for each of the precursors with these mole ratios, there is a declining trend of dispersion with the increase of reduction temperature. Evidently, the concentration of Mg in these precursors is insufficient to prevent the aggregation of Ni particles, as the reduction temperature exceeds 300 °C. For those with higher Mg to Ni mole ratios (0.2 and 0.4), the dispersion values for low-temperature reduction are lower than those on higher temperatures. Obviously, the hindering effect of Mg on nickel species reducibility is more expressed in precursors with higher Mg to Ni ratios. Shifting maximum dispersion values of Ni to higher reduction temperatures, besides the hindering effect of Mg on lower reduction temperatures, also reveals the protective function of Mg towards Ni aggregation at higher reduction temperatures. This observation can also be seen in the TPR profiles, as these precursors, shown in Figure 5b, do have a high temperature shoulder and a shifted maximum compared to other Mg modified precursors.

The hydrogen chemisorption study showed that the dispersion of nickel obtained in the studied reduced precursor systems depends on the nickel content in precursors, the loading of the metal modifier and support, but also on the temperature on which these catalyst precursors were reduced. The influence of porosity and dispersion degree, as well as their overall correlation, on catalytic activity in the process of hydrogenation of vegetable oils is still an active topic [47]. The question of obtaining an active catalyst remains open until the analyses of catalytic tests are performed.

Catalytic tests

Catalyst with the lowest nickel content modified with magnesium (Mg-0.25Ni/PF) was chosen to investigate the influence of precursor reduction temperature on its activity. The reduction temperature range of the precursor was determined based on its results from chemisorption measurements of reduced precursors that also included the temperature of 390 °C. Catalytic tests were performed by constant nickel to vegetable oil mass ratio of 0.03%. The refractive index and hydrogen consumption as a function of hydrogenation time are shown in Figure 6. Partial hydrogenation ending time for all tests was chosen for the values of the refractive index closer to 1.45500, which corresponds to the overall hydrogen consumption of 60 L (reducing the iodine value by approx. 80).

By increasing the reduction temperature, the activity of catalysts increases, reaching its maximum in the region 330-360 °C after which activity drastically starts decreasing. It is clear that these differences in activity cannot be interpreted in differences between dispersion degrees shown in Table 3. In addition, it would seem that the applied synthesis method is so robust that, although there are considerable differences between dispersion degrees, it produces catalysts with approximately the same activity for the temperature reduction region of 330-360 °C (Figure 6).

By the means of avoiding limiting temperature values in this region, the precursor reduction temperature was chosen to be 345 °C, which was then used as a reduction temperature in analysis of all catalysts with different nickel and magnesium content on hydrogenation activity. As to our knowledge, there is no report of the precursor reduction temperature below 400 °C, on SiO_2 support, for obtaining active catalysts used in vegetable oil hydrogenation process [10,48–54].

Although the comparison of catalytic activity, as a new type of support is introduced, can be hard to compare with literature results due to different reaction conditions, using the fall of iodine value can give some insight. The examples can be seen in the following works on different supports [10,50,55]. The most similar comparison can be seen in the work [56] on diatomite support, although the work was done on soybean oil. Beside the direct comparison with other data under the same conditions, it is obvious in Figure 6 that the catalyst is very active. Catalysts exhibit higher activity because of the availability of Ni on perlite support. Such intimate contact may favor a very close contact with the hydrogen gas; therefore, more hydrogen could be adsorbed on the catalysts, which in turn enhanced its hydrogenation activity.

For the series of catalytic tests shown in Figure 6, the sequence can be established for the catalyst in a specified time of the hydrogenation process. Order and activity ratio of different catalysts differ before and after 30 min for a partial hydrogenation process (most obviously seen for reduction temperatures of

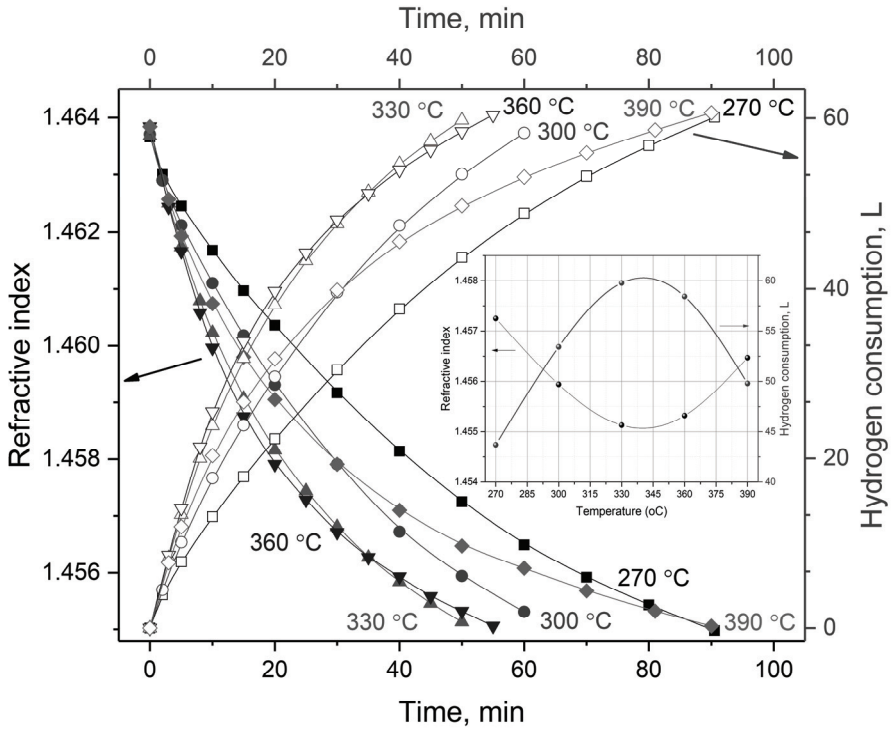

Figure 6. Influence of reduction temperature on catalytic activity for Mg-0.25Ni/PF (insert hydrogen consumption and refractive index value at 45 minute of hydrogenation time).

300 and 390 °C). In batch and semi-batch reactors, for the same reaction parameters, catalyst activity depends on the number of active sites, their accessibility and triacylglycerol composition during the catalytic hydrogenation of vegetable oils. Except in the case of catalyst deactivation, the number of active sites remains unchanged in reaction time. Accessibility of active sites can be, and triacylglycerol composition always is, a value that changes as hydrogenation process progresses. Therefore, different orders of established catalyst activities as a function of time indicate a various reaction pathway of catalysts prepared at different temperatures.

The influence of different nickel content in the catalysts on their activity is presented in Figure 7a. Because of the high activity of catalyst Mg-0.25Ni/PF used in preliminary tests, in order to obtain a wider distribution of results, nickel to vegetable oil mass ratio had to be reduced to 0.015%.

Hydrogen consumption shows that by increasing the nickel content, catalyst activity decreases. This can be expected according to the chemisorption measurements for catalysts up to Mg-0.75Ni/PF, which shows a slight decrease in the dispersion degree. As for catalysts with a higher nickel content (Mg-1.00Ni/PF and Mg-1.75Ni/PF), catalyst activity continues to decrease, although the dispersion degree is slightly higher than the previous one, and among the same values.

A possible explanation involves the existence of diffusion limitations for triacylglycerol molecules during the hydrogenation process in the system of partially reduced nickel basic carbonate. A typical triglyceride molecule has a diameter of approximately 5.8 nm [57] that can hamper access to Ni sites formed during the reduction process. On the other hand, with H_2 molecules, which have significantly smaller dimensions, these limitations are nonexistent during the chemisorption measurement, resulting in the differences of dispersion values and catalytic activity. It is worth noting that even the catalyst with the highest Ni content (Mg-1.75Ni/PF) is not inactive, which means that there are active Ni sites available to triacylglycerols.

The magnesium influence on catalytic activity for a constant mole ratio of nickel to SiO_2 is shown in Figure 7b. For comparison, a catalytic test performed using a catalyst without magnesium (0Mg-Ni/PF) with a same mole ratio of Ni:SiO_2 as in the test series is also shown.

By adding even the smallest amount of Mg during the synthesis, the catalytic activity significantly increases. With further increase of Mg content in the catalyst, activity increases, attaining the highest value for the mole ratio Mg:Ni = 0.1. Above this value,

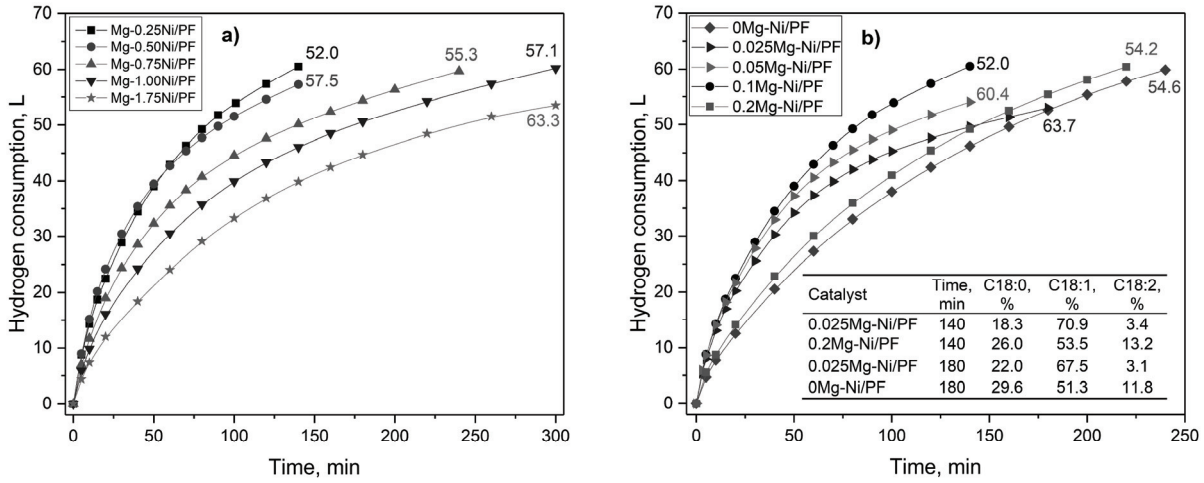

Figure 7. Catalytic activity for: a) influence of Ni content and b) influence of Mg content (numbers represent the final iodine value of partially hydrogenated sunflower oil).

despite the increase in the measured values of the dispersion of nickel, catalyst activity significantly decreases.

Change in order of catalyst activity as a function of observation time, noted in the analysis of the reduction temperature influence (Figure 6) can also be recognized for the catalyst 0.025Mg-Ni/PF compared to the catalysts 0Mg-Ni/PF and 0.2Mg-Ni/PF (Figure 7b). This change in catalytic activity order could suggest a different reaction pathway for observed catalysts. The results of fatty acid composition of partially hydrogenated oil for the same activity of two pairs of catalysts (0.025Mg-Ni/PF *vs*. 0.2Mg-Ni/PF in 140 min and 0.025Mg-Ni/PF vs. 0Mg-Ni-PF in 180 min) confirm a distinctly higher C18:1 selectivity compared to the other two (Table in Figure 7b). The overall increase in C18:1 fatty acid composition for partial hydrogenation, catalyst 0.025Mg-Ni/PF is 64% higher than both 0.2Mg-Ni/PF and 0Mg-Ni/PF.

CONCLUSION

Using the precipitation-deposition method on perlite as support, an active nickel-based catalyst modified with magnesium for hydrogenation of vegetable oil can be made.

Material differences, considering the change in morphology, texture and structure, due to the overall nickel and magnesium content, and after all the reducibility of supported precursors and dispersion of Ni in reduced precursors was established.

The morphological study confirmed successfully deposited nickel-magnesium species on the broken perlite honeycomb-like structure, nickel basic carbonate species dominantly and species that interact with the support, confirmed with FTIR and DR UV-Vis analysis, but also with TPR measurements.

With the increase in magnesium content, the influence is in favor of Mg modification up to a certain point on catalytic activity.

Using the reaction of hydrogenation of sunflower oil, it was established that the activity of catalysts strongly depends on the reduction temperature of precursors. For the selected reduction temperatures of 345 °C, the most active catalyst was obtained for mole ratios nickel to silica of 0.25 and magnesium to nickel 0.1.

The results of high nickel dispersion obtained by hydrogen chemisorption measurements compared to catalytic activity do not necessarily show positive correlation, which is contributed by diffusion limitations of triacylglycerols in the hydrogenation reaction process.

Acknowledgements

This work is supported by the Ministry of Education, Science and Technological Development of the Republic of Serbia (Grant No. III 45001).

REFERENCES

[1] M. Alkan, M. Doğan, J. Colloid Interface Sci. **207** (1998) 90-96

[2] A. Sarı, A. Karaipekli, Mater. Chem. Phys. **109** (2008) 459-464

[3] D. Acosta, J. Martinez, C. Carrera, E. Erdmann, E. Gonzo, H. Destefanis, Lat. Am. Appl. Res. **36** (2006) 317--320

[4] E. Kolvari, N. Koukabi, M.M. Hosseini, J. Mol. Catal,. A: Chem. **397** (2015) 68-75

[5] R. Jahanshahi, B. Akhlaghinia, RSC Adv. **5** (2015) 104087-104094

[6] A. Ramazani, M. Rouhani, E. Mirhadi, M. Sheikhi, K. Ślepokura, T. Lis, Nano. Chem. Res. **1** (2016) 87-107

[7] M. Balakos, E. Hernandez, Catal. Today **35** (1997) 415-425

[8] A. Wright, A. Wong, L. Diosady, Food Res. Int. **36** (2003) 1069-1072

[9] M. Fernandez, G. Tonetto, G. Crapiste, D. Damiani, J. Food Eng. **82** (2007) 199-208

[10] S.M. Echeverria, V.M. Andres, Appl. Catal. **66** (1990) 73--90

[11] M.P. Gonzalez-Marcos, J.I. Gutierrez-Ortiz, C. Gonzalez de Elguea, J.R. Gonzalez-Velasco, J. Mol. Catal., A: Chem. **120** (1997) 185-196

[12] J.R. Sohn, Catal. Today **73** (2002) 197-209

[13] J. Krstić, N. Vukelić, Z. Nedić, A. Milutinovic-Nikolić, A. Šućurović, D. Jovanović, Mater. Sci. Forum 494 (2005) 333-338.

[14] K. Ghuge, A. Bhat, G. Babu, Appl. Catal., A 103 (1993) 183-204.

[15] M. Gabrovska, D. Nikolova, J. Krstic, M. Stanković, P. Stefanov, R. Edreva-Kardjieva, D. Jovanović, Russ. J. Phys. Chem. A 83 (2009) 1461-1467.

[16] C.H. Bartholomew, Catal. Lett. 7 (1990) 27-51.

[17] D.G. Mustard, C.H. Bartholomew, J. Catal. 67 (1981) 186-206.

[18] J.W.E. Coenen, Stud. Surf. Sci. Catal. 3 (1979) 89-111.

[19] J.W.E. Coenen, B.G. Linsen, in: B.G. Linsen, J.M.H. Fortuin, C. Okkerse, J.J. Steggerda (Eds.), Physical and Chemical Aspects of Adsorbents and Catalysts, Academic Press, London and New York, 1970, pp. 471-527

[20] J.W. Coenen, Appl. Catal. **54** (1989) 65-78

[21] J.W. Coenen, J. Am. Oil Chem. Soc. **53** (1976) 382-389

[22] M. Gabrovska, J. Krstić, P. Tzvetkov, K. Tenchev, M. Shopska, N. Vukelić, D. Jovanović, Russ. J. Phys. Chem., A **85** (2011) 148

[23] P. Burattin, M. Che, C. Louis, J. Phys. Chem., B **101** (1997) 7060-7074.

[24] P. Burattin, M. Che, C. Louis, J. Phys. Chem., B **103** (1999) 6171-6178

[25] P. Burattin, M. Che, C. Louis, J. Phys. Chem., B **102** (1998) 2722-2732

[26] P. Kubelka, F. Munk, Z. Tech. Phys. **12** (1931) 593-601

[27] V.A. Drozdov, V.B. Fenelonov, L.G. Okkel, T.I. Gulyaeva, N.V. Antonicheva, N.S. Sludkina, Appl. Catal., A **172** (1998) 7-13

[28] D. Monti, A. Baiker, J. Catal. **83** (1983) 323-335

[29] J. Krstić, M. Gabrovska, D. Lončarević, D. Nikolova, V. Radonjić, N. Vukelić, D.M. Jovanović, Chem. Eng. Res. Des. **100** (2015) 72-80

[30] V. Radonjić, J. Krstić, D. Lončarević, D. Jovanović, N. Vukelić, M. Stanković, D. Nikolova, M. Gabrovska, Russ. J. Phys. Chem., A **89** (2015) 2359-2366

[31] A. Packter, S.C. Uppaladinni, Cryst. Res. Technol. **21** (1986) 51-58

[32] G. Pilatos, M. Samouhos, P. Angelopoulos, M. Taxiarchou, C. Veziri, R. Hutcheon, P. Tsakiridis, A.G. Kontos, Chem. Eng. J. **291** (2016) 106-214

[33] H. Allameh-Haery, E. Kisi, J. Pineda, L.P. Suwal, T. Fiedler, Powder Technol. **310** (2017) 329-342

[34] H.E. Rizk, I.M. Ahmed, S.S. Metwally, Chem. Eng. Process. **124** (2017) 131-136

[35] K. Hadjiivanov, M. Mihaylov, D. Klissurski, P. Stefanov, N. Abadjieva, E. Vassileva, L. Mintchev, J. Catal. **185** (1999) 314-323

[36] F. Farges, M. Munoz, R. Siewert, V. Malavergne, G.E. Brown, H. Behrens, M. Nowak, P.-E. Petit, Geochim. Cosmochim. Acta **65** (2001) 1679-1693

[37] W. Wang, M. Song, Z.Y. Zhang, M. Richardson, J. Non-Cryst. Solids **352** (2006) 2180-2186

[38] D. Brühwiler, H. Frei, J. Phys. Chem., B **107** (2003) 8547--8556

[39] P. Kukula, L. Červený, Appl. Catal., A **223** (2002) 43-55

[40] W.K.W. Lee, J.S.J. van Deventer, Langmuir **19** (2003) 8726-8734

[41] M.A. Ermakova, D.Y. Ermakov, Appl. Catal., A **245** (2003) 277-288

[42] M. Thommes, K. Kaneko, A. V. Neimark, J. P. Olivier, F. Rodriguez-Reinoso, J. Rouquerol, K. S. Sing, Pure Appl. Chem. **87** (2015) 1051-69

[43] Z. Cheng, Q. Wu, J. Li, Q. Zhu, Catal. Today **30** (1996), 147-155

[44] A. Iriondo, V. L. Barrio, J. F. Cambra, P. L. Arias, M. B. Güemez, R. M. Navarro, J. L. G. Fierro, Top. Catal. **49** (2008) 46-58

[45] M.A. Vannice, J. Catal. **44** (1976) 152-162

[46] R. A. Johnstone, A. H. Wilby, I. D. Entwistle, Chem. Rev. **85** (1985) 129-170

[47] J. Su, J. Chen, Microporous Mesoporous Mater. **237** (2017) 246-259

[48] J. Gusmao, D. Brodzki, G. Djéga-Mariadassou, R. Frety, Catal. Today **5** (1989) 533-544

[49] J.A. Anderson, M.T. Rodrigo, L. Daza, S. Mendioroz, Langmuir **9** (1993) 2485-2490

[50] J. Esmaeili, F. Rahimpour, Int. J. Hydrogen Energy **42** (2017) 24197-24204

[51] E. Kordouli, L. Sygellou, C. Kordulis, K. Bourikas, A. Lycourghiotis, Appl. Catal., B **209** (2017) 12-22

[52] S. Chen, C. Miao, Y. Luo, G. Zhou, K. Xiong, Z. Jiao, X. Zhang, Renew. Energy **115** (2018) 1109-1117

[53] E. Ramayeni, B.H. Susanto, D.F. Pratama, 2nd international Tropical Renewable Energy Conference, in IOP Conference Series: Earth and Environmental Science, island of Bali, Indonesia, 2018, p. 012055

[54] J. Farmani, M. Hamedi, M. Safari, A. Madadlou, Food Chem. **102** (2007) 827-833.

[55] D. Jovanovic, R. Radovic, L. Mares, M. Stankovic, B. Markovic, Catal. Today **43** (1998) 21-28

[56] M. Stanković, Ž. Čupić, M. Gabrovska, P. Banković, D. Nikolova, D. Jovanović, React. Kinet. Mech. Catal. **115** (2015) 105-127

[57] K. Jacobson, R. Gopinath, L.C. Meher, A.K. Dalai, Appl. Catal., B **85** (2008) 86-91.

VOJKAN D. RADONJIĆ[1]
JUGOSLAV B. KRSTIĆ[1]
DAVOR LONČAREVIĆ[1]
NIKOLA VUKELIĆ[2]
DUŠAN M. JOVANOVIĆ[1]

[1]Univerzitet u Beogradu, IHTM-Centar za katalizu i hemijsko inžinjerstvo, Beograd, Srbija
[2] Univerzitet u Beogradu, Fakultet za fizičku hemiju, Beograd, Srbija

NAUČNI RAD

Mg-Ni NA PERLITNOM NOSAČU KAO HIDROGENIZACIONI KATALIZATOR: UTICAJ SADRŽAJA Mg I Ni

Proučavana je moguća upotreba ekspantiranog perlita, oblika lomljenog pčelinjeg saća, kao nosača magnezijum modifikovanog niklenog katalizatora u procesu parcijalne hidrogenizacije suncokretovog ulja. Primenom precipitaciono-depozicione metode, sintetisane su dve grupe prekursora: različitog molskog odnosa Ni/SiO_2 sa konstantnim Mg/Ni molskim odnosom 0,1 i različitog Mg/Ni molskog odnosa sa konstantnim Ni/SiO_2 molskim odnosom 0,25. Izvršena je karakterizacija prekursora (skenirajuća elektronska mikroskopija, difuziona refleksiona ULj-Vid, infracrvena spektroskopija, N_2-fizisorpcija, temperaturski programirana redukcija - TPR i He-piknometrija) u cilju utvrđivanja razlika u materijalu, uzimajući u obzir promene u morfologiji, strukturi, teksturi i reducibilnosti ukupnog sadržaja Ni i Mg. Dodatno, TPR i hemisorpcija vodonika urađene su u cilju procene opsega temperature redukcije prekursora i stepena disperzije nikla u redukovanim prekursorima. Utvrđeno je postojanje interakcija između Ni^{2+} i perlitnog nosača, a dokazana je za različite reducibilnosti i disperznosti kao funkcija Ni/SiO_2 i Mg/Ni molskog odnosa. Nakon redukcije prekursora i impregnacije parafinskim uljem, dobijeni katalizatori su testirani u reakciji hidrogenizacije suncokretovog ulja. Katalitička aktivnost je praćena padom indeksa refrakcije i potrošnjom vodonika. Utvrđeno je da na katalitičku aktivnost dominantan uticaj ima dostupnost aktivnih Ni^0 centara molekulima triacilglicerola, a ne njihov stepen disperzije utvrđen vodonikom.

Ključne reči: hidrogenizacija; magnezijum; nikleni katalizator; perlit; redukcija.